Rainfall-induced ground deformation in southern Africa

Olivier Dauteuil, Marc Jolivet, Louis Gaudaré, Anne-morwenn Pastier

RESEARCH ARTICLE

Rainfall-induced ground deformation in southern Africa

Olivier Dauteuil[1] | Marc Jolivet[1] | Louis Gaudaré[1] | Anne-Morwenn Pastier[2]

[1]Géosciences-Rennes, UMR-CNRS 6118, University of Rennes, 35042, Rennes, France

[2]Helmholtz-Zentrum Potsdam—Deutsches GeoForschungsZentrum, 14473, Potsdam, Germany

Correspondence
Olivier Dauteuil, Géosciences-Rennes, UMR-CNRS 6118, University of Rennes, 35042 Rennes, France.
Email: olivier.dauteuil@univ-rennes1.fr

Funding information
Conseil National de la Recherche Scientifique; Université de Rennes

Abstract

We present an analysis of ground deformation induced by large-scale seasonal rainfall in Southern Africa, based on GPS and GRACE time series and on simulations of elastic flexural response to hydrological loading. This large-scale study including South Zambia, South Angola, North Namibia and North Botswana displays a latitudinal precipitation gradient between tropical to semi-arid conditions. GRACE data display annual variations in water mass decreasing drastically southwards. GPS time series of three permanent stations located in Zambia, Namibia and Botswana show seasonal synchronous vertical displacements with amplitude decreasing southwards from 4 to 2 cm, with a shift of 2–3 months from the main rainfall season. Flexure simulations integrating rainfall, evapotranspiration, water storage, flood migration and river output produce a ground flexure up to 6 cm with timing in agreement with the GPS time series. It highlights the hydrological buffering of surface aquifer located in the Kalahari sands.

KEYWORDS
Hydrology, elastic flexure, rainfall, ground deformation

1 | INTRODUCTION

The Earth surface deforms under several processes involving both deep earth and external envelopes, such as ocean, atmosphere and continental water (Biessy et al., 2011; Cazenave & Feigl, 1994). The dynamics of the external envelopes generate variations in mass recorded by GNSS methods (Ray et al., 2013; Ruttner et al., 2022; White et al., 2022), ground gravimetry (Crossley et al., 2005; Güntner et al., 2017) and spatial gravimetry (Ramillien et al., 2008; Wahr et al., 2004). The regional-scale hydrology is investigated from GRACE satellite data where gravity variations are converted into an equivalent water thickness and into displacements (Chanard et al., 2018; Llovel et al., 2010; Ramillien et al., 2008; Wahr et al., 2004). GRACE data were combined to GPS time series to estimate the atmosphere and non-tidal ocean loading at regional scale (Fu et al., 2012; Nahmani et al., 2012). Few works investigate the impact of rainfall on the ground deformation at the regional scale. Studies described punctual effects of extreme events on ground deformation: heavy rainfalls and typhoons can generate a ground subsidence around 1 cm for daily precipitation of 5–10 mm/day in Western Africa (Nahmani et al., 2012) of some cm for variations in precipitations of 15 cm per month in Australia (Li et al., 2020). However, few regional-scale studies investigate the ground deformation of an area submitted to seasonal high-rainfall gradients, such as transition areas between sub-tropical and semi-arid climates. Such transitional regions undergo cyclic hydrological loads of which regional gradients can be important as in Northern Australia, India, Eastern Asia, Southern Sahara and Southern Africa. We focused our ground deformation study on Southern Africa (Figure 1): unlike India and Eastern Asia, this region is located in an intraplate setting, that is, away from main geodynamic activities sand from oceanic and earth tides.

2 | SOUTHERN AFRICAN SETTINGS

Southern Africa is a steady region where the water resources are driven by annual precipitations that display high gradients (Figure 1): some tens of mm/year on the Namibian coast to more than 1300 mm/year in the Democratic Republic of Congo. GRACE data (Krogh et al., 2010) highlight these contrasted variations in equivalent water thickness (Figure 1): the amplitude of annual variations ranges from 30 to 50 cm north of 20° S and decreases to less than 10 cm in the South. This latitudinal contrast is abrupt and localized at a latitude of 20° S. GPS time series of three stations located in Maun (Botswana), Rundu (Namibia) and Mongu (Zambia) (Figure 1) display seasonal vertical variations from 2 cm in Maun to 40 cm in Mongu (Pastier et al., 2017; Pastier, 2018). The three stations display in-phase vertical displacements decreasing in magnitude towards the south revealing that they record the same loading process whose impact fades southwards. This variation in ground deformation is anti-correlated with the water equivalent thickness: the maximum in GPS time series fit to the minimum of GRACE time series, and vice versa. Thus, an increase in water loading generates a ground subsidence. The Southward decrease in the amplitude of the ground deformation and the synchronicity between the three stations indicate that these displacements are generated by water loading in Angola and Zambia where the regional precipitations are maximum (Figure 1, S1). We will further explore this mechanism through numerical simulations of a flexure response to a hydrological load in the area including southern Angola, Zambia, northern Namibia and Botswana.

Statement of significance

We investigate the impact of the annual rainfall on the ground deformation in Southern Africa (Angola, Zambia, Namibia and Botswana). GPS time series record annual variations of vertical displacements of the ground surface up to 4 cm, correlated to changes in water mass recorded by GRACE data. Simulations of the ground surface displacements integrating complete hydrological budget with rainfall, water export and temporary water storage show centimetre vertical displacements decreasing southwards. The maximum of downward displacements occurs 2 months after the main rainfall period, as recorded by GPS stations. This time offset is due to the permeability of the Kalahari sand and the flat topography of this region that slow down the water propagation.

3 | HYDROLOGICAL BUDGET

The hydrological budget driving the water load in a given area results in the difference between the input due to local rainfall and incoming rivers, and the outputs through evapotranspiration and fluvial export outside. We used precipitation data from the WorldClim database (Fick & Hijmans, 2017) that provides monthly rainfalls in cell size of 2.5 min (Figure S1). The maximum of precipitations occurs from October to March: up to 300 mm in North Zambia, East and West Angola, and the minimum (less than 25 mm/month) in
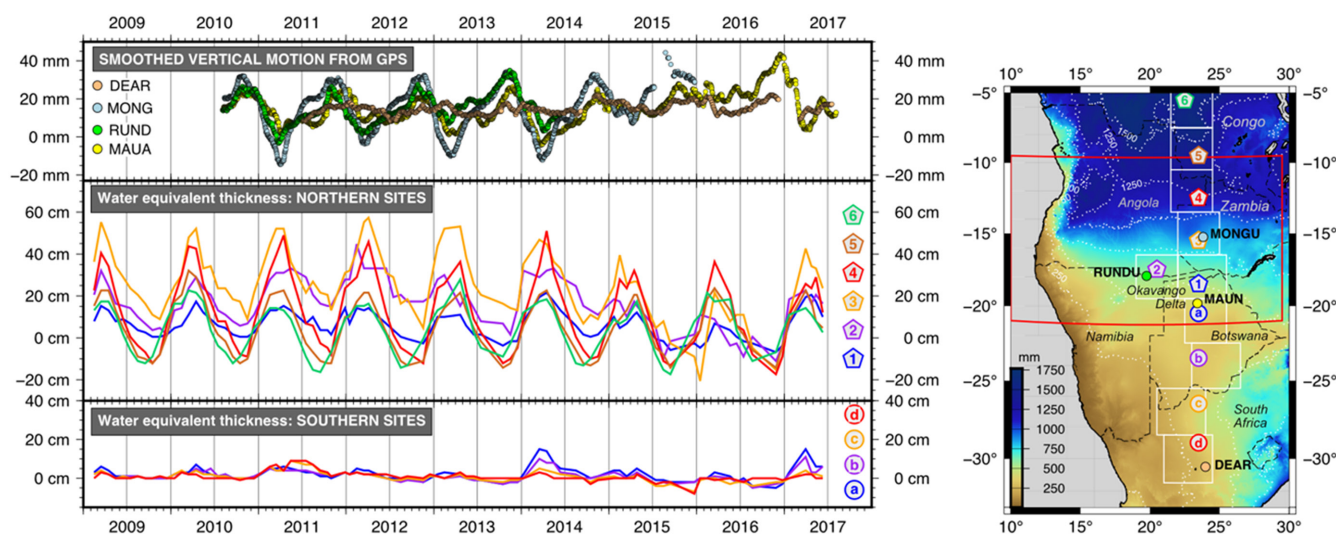

FIGURE 1 Hydrological variations from GRACE data and ground deformation from GPS in Southern Africa. To the right, the precipitation map (data from WorldClim website) shows the location of the GRACE tiles used in this study (white rectangles, data from GRACE Tellus site) and of the GPS stations (circles, Maun in green, Rundu in red, Mongu in blue) (Pastier et al., 2017). The red rectangle limits the study area. The left middle and lower plots show the variations in water equivalent thickness deduced from GRACE from February 2009 to November 2017 on sites located North and South of Maun (Botswana): the variations within the northern sites range up to 60 cm while they vary up to 20 cm to the South. Note the lack of significant linear trend revealing the absence of water storage or water release during the considered period. The left upper plot shows the GPS-measured variations in vertical ground deformation at the three stations (18). Note the anti-correlation between soil deformation and hydrological variations.

May, June and July in the whole study area. An exhaustive and accurate quantification of the outputs at such a regional scale is difficult to estimate because of the lack of realistic evapotranspiration data. Evapotranspiration is only measured locally in some limited areas such as the Okavango Delta (Bauer et al., 2004; Moses & Hambira, 2018) and no data are available in Angola. To bypass this difficulty, a potential evapotranspiration (PET) is modelled by integrating a set of climatic parameters (McCabe et al., 2015). It provides a theoretical maximum amount of water exported by physical evaporation and vegetation activity assuming an infinite water availability. In our study area, the annual PET provided by the WorldClim database (Fick & Hijmans, 2017) (Figure S2) is larger than the annual rainfall, indicating that, in theory, no water must flow outside the study area. A simple calculation of monthly hydrological budget by subtracting the PET from the rainfall (Figure S3) shows a huge deficit in water up to 290mm during some summer months. Only Angola and Zambia regions display a water excess from November to March, up to 184mm in December. Therefore, the theoretical PET cannot be integrated in the hydrological budget to estimate the variations in effective water load. Thus, to estimate the monthly change in water mass, we used a simple formulation:

$$Wv_m = (Prec_m + Ws_{m-1}) \cdot Cout \qquad (1)$$

where at a given month ($_m$), the water mass (Wv_m) results in the month precipitation ($Prec_m$) plus the water locally stored from the previous month (Ws_{m-1}), multiplied by an effective coefficient (Cout) that gathers all the processes exporting water from the area (evaporation, transpiration and rivers). This coefficient was estimated empirically by assuming that the water mass at a given month cannot be greater than the rainfall mass plus the water stored during the previous month. Therefore, Cout ranges from 0 (all the water is exported from the given region) to 1 (all the water is stored inside the given region) (Figure 2). Cout=1 is not consistent with GRACE data that indicate none or weak water storage as shown in Figure 1. Calculations based on Equation 1 show that the maximum of water

present in the zone occurs in March, while the maximum of rainfall occurs in December and in January, that is, a time lapse of 3months (Figure S5). To constrain this output coefficient, we also considered the range of flexure that affects the entire study area (Figure 2). As expected, the amplitude of flexure increases as Cout increases, that is, when the loading increases. For Cout values of 0.25, 0.5 and 0.75, the maximum of flexure happens in March, and the minimum in September. Considering the flexure amplitude recorded by the GPS station, Cout should range from 0.25 to 0.5, meaning that the evapotranspiration and river export extract three quarters to half of the water from the study area. The following simulations were done using a realistic Cout value of 0.5.

The water mass remaining from the previous month (Ws_{m-1}) includes the water stored in subsurface aquifers and the water flowing in the rivers, not yet exported outside the study area. The high permeability and high porosity of the unconsolidated Kalahari sands coupled with a flat topography (regional slope less than 0.1%) slow down the water flow in the rivers and generate annual floods out of phase with local rainfalls. The water leaving the study area through the river is not considered because it no longer contributes to the overall hydrological mass.

The study area includes the endorheic Okavango Delta in north Botswana (Figure 1), which temporarily stores water coming from the Angolan mountains; 96% of the water flowing to the fan disappears via evapotranspiration (Bauer et al., 2004; Gumbricht et al., 2004; McCarthy, 2006), the 4% remaining being evacuated in the small rivers. To estimate the monthly amount of water temporally stored in the fan, we compared the amount of rainfall in the upstream watershed to the water discharge measured at the town of Mohembo, located at the entrance of the Okavango Delta. The discharge data at Mohembo were downloaded from the Okavango Research Institute's database. The annual volume of rainfall in the watershed reaches 147.04km^3 and the volume flowing at Mohembo is 9.22km^3, that is, only 6% of the rainfall flows at Mohembo. We integrated the water temporally stored in the Okavango Delta by adding 6% of the precipitations falling in the
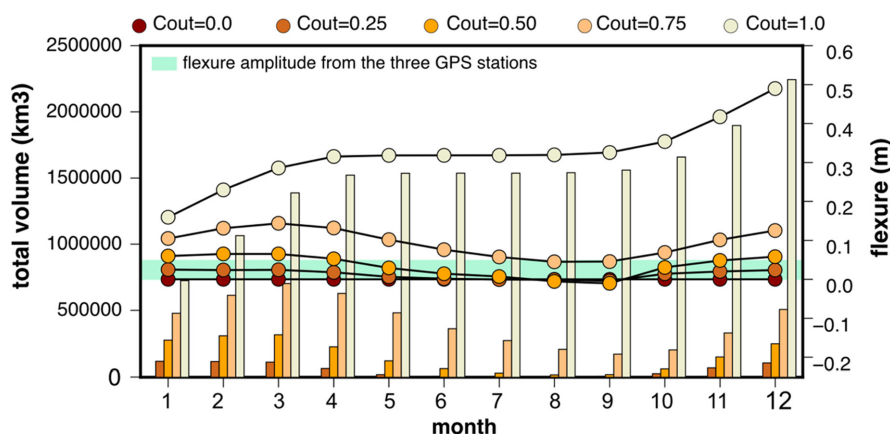

FIGURE 2 Impact of water output coefficient (see text) on the total volume of water in the study area (vertical bars) and on the flexure amplitude (lines and dots). Five values were tested: 0.0, 0.25, 0.5, 0.75 and 1.0 (0 means that all the water exits the area, 1 all the rainfall is stored). The light-green rectangle defines the flexure amplitude recorded by the three GPS stations. The coefficient values between 0.25 and 0.5 seem to be the most realistic for the study area.

Angolan part of the Okavango watershed to the area of the Delta, with a delay of 2 months.

Finally, the hydrological budget is described as follows:

$$Wv_m = (Prec_m + Ws_{m-1})^* Cout + Wdo_m \qquad (2)$$

Wdo_m is the water stored temporally in the Okavango Delta. This formula provides a monthly hydrological budget displayed in Figure S5. Three simulations were processed corresponding to different hydrological settings: (i) a loading only from rainfall without output (Figure S6), (ii) a loading from rainfall corrected for stored water and output coefficient and (iii) a loading from rainfall corrected for stored water, output coefficient and water stored in the Okavango Delta (Figure S7). All the simulations were processed with Cout = 0.5.

4 | FLEXURE SIMULATION

The amplitude of a loading flexure of the lithosphere is driven by the vertical load, the whole rheology of the lithosphere which is integrated by the effective elastic thickness (Te), the Young Modulus and Poisson coefficient. Te is the most critical value but complex to estimate (Watts & Burov, 2003): it depends on the crustal thickness, its composition and the depth of the lithosphere. In the study area, Te ranges from 10 km close to the shoreline up to 120 km below the Kalahari and Congo cratons (Pérez-Gussinyé et al., 2009). We used the code gFlex (Fick & Hijmans, 2017) to simulate the 2D flexure, taking into account the spatial variability of Te. The elastic flexure was estimated with Finite Differences solution and free vertical translation at the plate boundaries. The Young's modulus is 6.5 10¹⁰ Pa and Poisson's ratio is 0.25. One calculation was processed over the whole study area for each month and the time evolution of three points was extracted: Maun, Rundu and Mungo that corresponds to sites with GPS time series. The results are displayed both in the supplementary files with the maps of the monthly flexure and in the main part of the article where the comparison with the three GPS stations is done.

5 | HYDROLOGICAL GROUND DEFORMATION

5.1 | Flexure from monthly rainfall

The first simulation evaluates the effect of monthly rainfall on the ground deformation (Figures 3 and S6). The ground reacts immediately to the water loading as expected from the elastic mechanical behaviour: the flexure reaches 8 cm in the northern and eastern parts of the study area. The maximum of displacement happens from December to January, when the rainfall is greater and no deformation is observed during the dry season from June to August. Between these two periods, the flexure amplitude decreases as the water loading diminishes. The variations in vertical displacements were followed in three places: Maun, Rundu and Mongu (Figure 3) where GPS time series are available. The displacements are synchronous in the three places: the
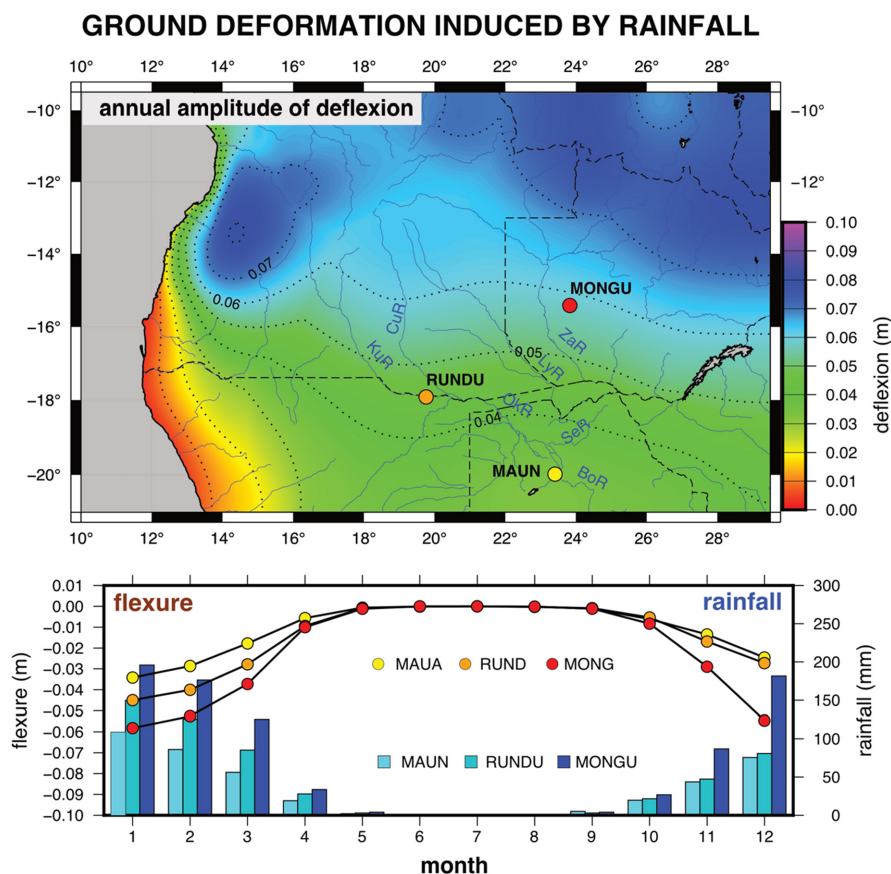

FIGURE 3 Flexure induced by rainfall loading. The upper map displays the annual range of vertical displacement. The dotted deflection curves are spaced every 1 cm. The lower plot illustrates the modelled monthly variation of vertical displacement of the three GPS sites, and the vertical bars illustrate the monthly rainfall at each site.

maximum is at Mongu (up to 5.8 cm in January) that is the closest site to the maximum of rainfall, and the minimum is at Maun (up to 3.3 cm in January), the farthest place to the maximum rainfall. The deformation is null for the three places from June to September. However, the magnitude of displacement is twice higher than recorded with GPS (Figure 1). The rainfall generates a cm-scale deflection synchronous to the water loading with an order of magnitude of the displacements being similar to the measured data, but not with the good timing.

5.2 | Flexure from complete hydrological budget

The second simulation integrates the evapotranspiration, the river export outside the study area and the water in the rivers located inside the study area (Figures 4 and S08). The loss of water mass compared to the rainfall mass results in a lowering of the flexure magnitude only reaching up to 6.2 cm. It also generates a time offset of 2 months: the maximum of flexure occurs from February to March, and the minimum from July to September (only August displays no flexure). Therefore, the rainfall and the flexure are not in phase, as observed in the measurements: the subsidence occurs even during the dry season due to the water migration and the water stored in aquifer. The three GPS stations (Figure 4) display similar behaviours, but the deformation in Mongu is twice higher than in Maun, and 1.5 higher than in Rundu. The displacements in Maun and in Mongu are close from October to December. The water storage inside the

Okavango Delta affects the deformation in Maun by slowing down the decrease of flexure and offsetting the maximum of flexure to March, instead of February.

5.3 | Crustal sensitivity to the hydrological loading

The numerical simulations of flexure response to water loading integrating mechanical behaviour of the crust highlight the sensitivity of the ground surface to water loading, even in an area assumed to be located above craton domains. Unfortunately, this effect is poorly considered in the regional-scale studies of ground deformation by GNSS methods (Silverii et al., 2016), while it can generate centimetres of vertical ground deformation. Only long, continuous time series can effectively characterize this effect by estimating its amplitude and periodicity, allowing to deconvolute the signal of ground displacement into different processes. However, a complete hydrological budget at the regional scale is complex to realize because many factors are involved. This large-scale study focused on a region with high precipitation and temperature gradients reveals the necessity to acquire in situ evapotranspiration data, to constrain the flowing rate in rivers depending on the regional slopes (<0.1% in the study area), and to estimate the water storage in the subsurface aquifers. The water storage corresponds to the water still present in the subsurface aquifers made up of the poorly consolidated, largely aeolian Kalahari sands (De Vries, 1984; Lekula et al., 2018). Because of its high porosity of
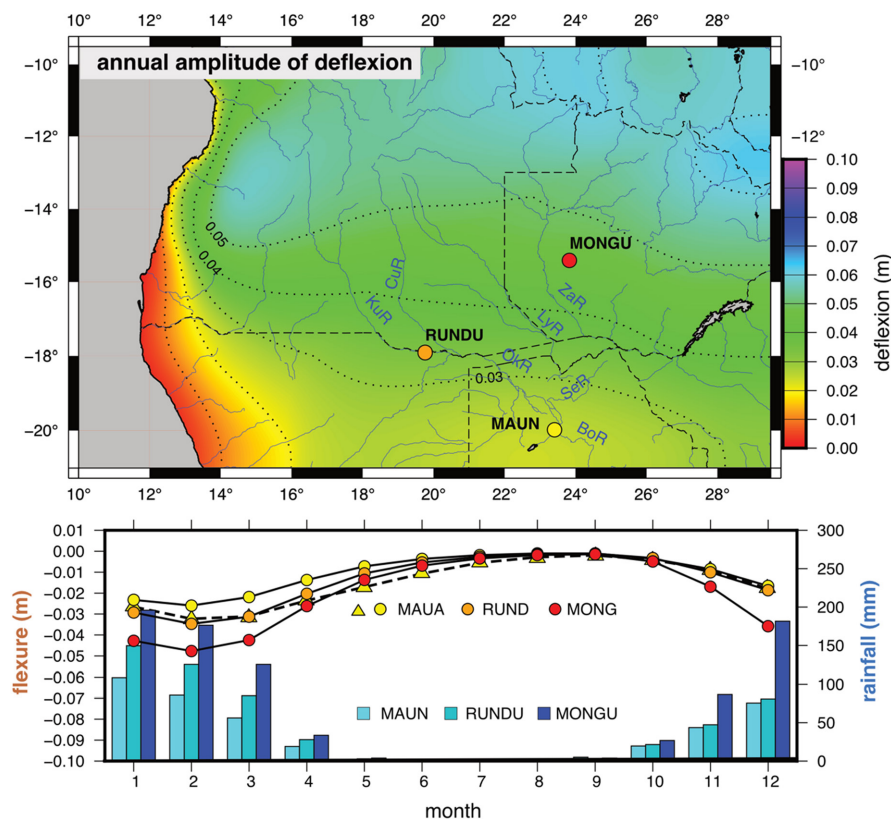

FIGURE 4 Flexure induced by water mass present in the study area. The hydrological budget integrates the rainfall and the water previously stored pondered by a coefficient (see text for explanation). The upper map displays the annual range of vertical displacement. The dotted deflection curves are spaced every 1 cm. The lower plot illustrates the monthly variations of vertical displacement of the three GPS sites, and the vertical bars illustrate the monthly rainfall at each site. The dashed line with yellow triangles shows the monthly flexure at Maun considering 6% of water storage in the Okavango Delta.

43–49% (Wang et al., 2007) and its high permeability, this type of aquifer stores a large amount of water during the rainy season before discharging in the rivers during the dry period, and are water buffers that largely regulate the water availability in that region.

6 | CONCLUSION

Southern Africa displays high-rainfall gradients from tropical climate to the North to semi-arid climate to the South. The precipitations integrated at a regional large scale represent a huge mass of water well recorded by GRACE, which load deforms the ground surface, as observed on GPS time series. The seasonal vertical movement up to several centimetres in magnitude is significant and should be considered in regional studies of ground deformation, especially in intraplate domain where no geodynamic process occurs. The record of the ground deformation allows constraining both the regional hydrology of Southern Africa and the crustal response to short-term–low amplitude stress. Similar studies should be realized in other intracontinental regions displaying contrasted rainfall distribution such as South America or India where the geodynamic context is stable.

DATA AVAILABILITY STATEMENT
Data sharing not applicable to this article as no datasets were generated or analysed during the current study.

ORCID
Olivier Dauteuil https://orcid.org/0000-0002-8814-8610
Marc Jolivet https://orcid.org/0000-0002-1160-9386

REFERENCES
Bauer, P., Thabeng, G., Stauffer, F., & Kinzelbach, W. (2004). Estimation of the evapotranspiration rate from diurnal groundwater level fluctuations in the Okavango Delta, Botswana. *Journal of Hydrology*, *288*, 344–355. https://doi.org/10.1016/j.jhydrol.2003.10.011

Biessy, G., Moreau, F., Dauteuil, O., & Bour, O. (2011). Surface deformation of an intraplate area from GPS time series. *Journal of Geodynamics*, *52*, 24–33.

Cazenave, A., & Feigl, K. (1994). Formes et mouvements de la terre. In *Formes et mouvements de la Terre—Satellites et géodésie*. CNRS Edition/Belin, 159 pp.

Chanard, K., Fleitout, L., Calais, E., Rebischung, P., & Avouac, J.-P. (2018). Toward a global horizontal and vertical elastic load deformation model derived from GRACE and GNSS Station position time series. *Journal of Geophysical Research: Solid Earth*, *123*, 3225–3237. https://doi.org/10.1002/2017JB015245

Crossley, D., Hinderer, J., & Boy, J.-P. (2005). Time variation of the European gravity field from superconducting gravimeters. *Geophysical Journal International*, *161*, 257–264. https://doi.org/10.1111/j.1365-246X.2005.02586.x

De Vries, J. J. (1984). Holocene depletion and active recharge of the Kalahari groundwaters—A review and an indicative model. *Journal of Hydrology*, *70*, 221–232. https://doi.org/10.1016/0022-1694(84)90123-9

Fick, S. E., & Hijmans, R. J. (2017). WorldClim 2: New 1-km spatial resolution climate surfaces for global land areas. *International Journal of Climatology*, *37*, 4302–4315. https://doi.org/10.1002/joc.5086

Fu, Y., Freymueller, J. T., & Jensen, T. (2012). Seasonal hydrological loading in southern Alaska observed by GPS and GRACE. *Geophysical Research Letters*, *39*, L15310. https://doi.org/10.1029/2012GL052453

Gumbricht, T., Wolski, P., Frost, P., & McCarthy, T. S. (2004). Forecasting the spatial extent of the annual flood in the Okavango delta, Botswana. *Journal of Hydrology*, *290*, 178–191.

Güntner, A., Reich, M., Mikolaj, M., Creutzfeldt, B., Schroeder, S., & Wziontek, H. (2017). Landscape-scale water balance monitoring with an iGrav superconducting gravimeter in a field enclosure. *Hydrology and Earth System Sciences*, *21*, 3167–3182. https://doi.org/10.5194/hess-21-3167-2017

Krogh, P. E., Andersen, O. B., Michailovsky, C. I. B., Bauer-Gottwein, P., Rowlands, D. D., Luthcke, S. B., & Chinn, D. S. (2010). Evaluating terrestrial water storage variations from regionally constrained GRACE mascon data and hydrological models over southern Africa—Preliminary results. *International Journal of Remote Sensing*, *31*, 3899–3912. https://doi.org/10.1080/01431161.2010.483483

Lekula, M., Lubczynski, M. W., & Shemang, E. M. (2018). Hydrogeological conceptual model of large and complex sedimentary aquifer systems—Central Kalahari Basin. *Physics and Chemistry of the Earth Parts A/B/C*, *106*, 47–62. https://doi.org/10.1016/j.pce.2018.05.006

Li, H., Wang, X., Wu, S., Zhang, K., Chen, X., Qiu, C., Zhang, S., Zhang, J., Xie, M., & Li, L. (2020). Development of an Improved Model for Prediction of Short-Term Heavy Precipitation Based on GNSS-Derived PWV. *Remote Sensing*, *12*, 4101. https://doi.org/10.3390/rs12244101

Llovel, W., Becker, M., Cazenave, A., Jcretaux, J.-F., & Ramillien, G. (2010). Global land water storage change from GRACE over 2002–2009; inference on sea level. *Comptes Rendus Geosciences*, *342*, 179–188.

McCabe, G. J., Hay, L. E., Bock, A., Markstrom, S. L., & Atkinson, R. D. (2015). Inter-annual and spatial variability of Hamon potential evapotranspiration model coefficients. *Journal of Hydrology*, *521*, 389–394. https://doi.org/10.1016/j.jhydrol.2014.12.006

McCarthy, T. S. (2006). Groundwater in the wetlands of the Okavango Delta, Botswana, and its contribution to the structure and function of the ecosystem. *Journal of Hydrology*, *320*, 264–282. https://doi.org/10.1016/j.jhydrol.2005.07.045

Moses, O., & Hambira, W. L. (2018). Effects of climate change on evapotranspiration over the Okavango Delta water resources. *Physics and Chemistry of the Earth Parts A/B/C*, *105*, 98–103. https://doi.org/10.1016/j.pce.2018.03.011

Nahmani, S., Bock, O., Bouin, M.-N., Santamaría-Gómez, A., Boy, J.-P., Collilieux, X., Métivier, L., Panet, I., Genthon, P., de Linage, C., & Wöppelmann, G. (2012). Hydrological deformation induced by the west African monsoon: Comparison of GPS, GRACE and loading models. *Journal of Geophysical Research: Solid Earth*, *117*, B05409. https://doi.org/10.1029/2011JB009102

Pastier, A.-M. (2018). The Okavango Delta through the deformation of its surface: Multi-proxy approach from hydrology to tectonics. *Thesis of Unversity of Rennes*, *1*, 148.

Pastier, A.-M., Dauteuil, O., Murray-Hudson, M., Moreau, F., Walpersdorf, A., & Makati, K. (2017). Is the Okavango Delta the terminus of the east African rift system? Towards a new geodynamic model: Geodetic study and geophysical review. *Tectonophysics*, *712–713*, 469–481. https://doi.org/10.1016/j.tecto.2017.05.035

Pérez-Gussinyé, M., Metois, M., Fernández, M., Vergés, J., Fullea, J., & Lowry, A. R. (2009). Effective elastic thickness of Africa and its relationship to other proxies for lithospheric structure and surface tectonics. *Earth and Planetary Science Letters*, *287*, 152–167. https://doi.org/10.1016/j.epsl.2009.08.004

Ramillien, G., Bouhours, S., Lombard, A., Cazenave, A., Flechtner, F., & Schmidt, R. (2008). Land water storage contribution to sea level from GRACE geoid data over 2003–2006. *Global and Planetary Change*, *60*, 381–392.

Ray, J., Griffiths, J., Collilieux, X., & Rebischung, P. (2013). Subseasonal GNSS Positioning Errors. *Geophysical Research Letters*, *40*, 5854–5860. https://doi.org/10.1002/2013GL058160

Ruttner, P., Hohensinn, R., D'Aronco, S., Wegner, J. D., & Soja, B. (2022). Modeling of residual GNSS station motions through meteorological data in a machine learning approach. *Remote Sensing*, *14*, 17. https://doi.org/10.3390/rs14010017

Silverii, F., D'Agostino, N., Métois, M., Fiorillo, F., & Ventafridda, G. (2016). Transient deformation of karst aquifers due to seasonal and multiyear groundwater variations observed by GPS in southern Apennines (Italy). *Journal of Geophysical Research: Solid Earth*, *121*, 8315–8337. https://doi.org/10.1002/2016JB013361

Wahr, J., Swenson, S., Zlotnicki, V., & Velicogna, I. (2004). Time-variable gravity from GRACE: First results. *Geophysical Research Letters*, *31*, L11501. https://doi.org/10.1029/2004GL019779

Wang, L., D'Odorico, P., Ringrose, S., Coetzee, S., & Macko, S. A. (2007). Biogeochemistry of Kalahari sands. *Journal of Arid Environments*, *71*, 259–279. https://doi.org/10.1016/j.jaridenv.2007.03.016

Watts, A. B., & Burov, E. (2003). Lithospheric strength and its relationship to the elastic and seismogenic layer thickness. *Earth and Planetary Science Letters*, *213*, 113–131.

White, A. M., Gardner, W. P., Borsa, A. A., Argus, D. F., & Martens, H. R. (2022). A review of GNSS/GPS in Hydrogeodesy: Hydrologic loading applications and their implications for water resource research. *Water Resources Research*, *58*, e2022WR032078. https://doi.org/10.1029/2022WR032078

SUPPORTING INFORMATION

Additional supporting information can be found online in the Supporting Information section at the end of this article.